

Validation of *in vivo* fluorochrome concentrations measured using fluorescence molecular tomography

Edward E. Graves

Stanford University School of Medicine
Department of Radiation Oncology
Stanford, California 94305 USA

Doreen Yessayan

Gordon Turner

Ralph Weissleder

Vasilis Ntziachristos

Massachusetts General Hospital
Harvard Medical School
Center for Molecular Imaging Research
Department of Radiology
Charlestown, Massachusetts 02129 USA
E-mail: vasilis@helix.mgh.harvard.edu

Abstract. Fluorescence molecular tomography (FMT) has emerged as a means of quantitatively imaging fluorescent molecular probes in three dimensions in living systems. To assess the accuracy of FMT *in vivo*, translucent plastic tubes containing a turbid solution with a known concentration of Cy 5.5 fluorescent dye are constructed and implanted subcutaneously in nude mice, simulating the presence of a tumor accumulating a fluorescent molecular reporter. Comparisons between measurements of fluorescent tubes made before and after implantation demonstrate that the accuracy of FMT reported for homogeneous phantoms extends to the *in vivo* situation. The sensitivity of FMT to background fluorescence is tested by imaging fluorescent tubes in mice injected with Cy 5.5-labeled Annexin V. For small tube fluorochrome concentrations, the presence of background fluorescence results in increases in the reconstructed concentration. This phenomenon is counteracted by applying a simple subtraction correction to the measured fluorescence data. The effects of varying tumor photon absorption are simulated by imaging fluorescent tubes with varying ink concentrations, and are found to be minor. These findings demonstrate the *in vivo* quantitative accuracy of fluorescence tomography, and encourage further development of this imaging modality as well as application of FMT in molecular imaging studies using fluorescent reporters. © 2005 Society of Photo-Optical Instrumentation Engineers. [DOI: 10.1117/1.1993427]

Keywords: fluorescence molecular tomography; fluorescent probes; diffuse optical tomography; molecular imaging.

Paper 04094RRR received Jun. 4, 2004; revised manuscript received Mar. 30, 2005; accepted for publication Apr. 4, 2005; published online Aug. 10, 2005.

1 Introduction

In vivo observation and imaging of living subjects using fluorescence is one of the most rapidly evolving fields in clinical and experimental biology. Fluorescent probes offer a number of practical advantages in that they are inexpensive, present straightforward synthetic and conjugation chemistries, and emit detectable, nonionizing photons on excitation. A variety of strategies have been developed to image specific cellular and biochemical events *in vivo* using targeted and/or activatable fluorochromes conjugated to biocompatible delivery vehicles suitable for systemic injection. Imaging of cell-surface receptors and antigens has been accomplished in animal models using fluorescently labeled antibodies and antibody fragments,^{1,2} proteins that bind cell-surface moieties,³ and peptides that bind to cell-surface receptors.^{4,5} Self-quenched fluorescent probes activated by specific proteolytic cleavage⁶ or specific nucleic acid binding⁷ have also been developed for *in vivo* use, allowing functional biochemical imaging of living subjects. Imaging of gene expression via fluorescence has been achieved using genetically encoded fluorescent reporters such as green fluorescent protein (GFP).⁸

With advances in fluorescent probe technology, corresponding improvements in fluorescence imaging have also been achieved. Fluorescence has historically been used as a means of contrast in microscopy,^{9–12} a technique that has also been applied to living subjects through the use of intravital windows.^{13,14} Photographic techniques such as fluorescence reflectance imaging (FRI) have been applied toward imaging macroscopic fluorescent signatures deeper in tissues.^{5,8,15–18} Such methods have offered a simple means of imaging the distribution and/or activation of fluorescent probes in living subjects, and can provide semiquantitative results when the sizes and tissue depths of the imaging targets are properly controlled. However, as FRI is a single projection technique, it is unable to provide fully quantitative results because of nonlinear depth-dependent photon absorption in the subject.^{19–21} To quantitatively image fluorescence in this situation, tomographic methods have been adopted. Hardware and software for *in vivo* fluorescence imaging have been developed, including means for localizing fluorophores in diffuse media^{22,23} as well as tomographically resolving fluorophore distributions,^{24–37} as demonstrated with simulated and phantom data. Recently, these techniques have been applied to the observation of protease activity³⁸ and of chemotherapeutic

Address all correspondence to Edward Graves, Radiation Oncology, Stanford University, 875 Blake Wilbur Dr., CC-G202, Stanford, CA 94305. Tel: 650-723-5591. Fax: 650-498-4015. E-mail: egraves@stanford.edu

action²¹ in mouse models. These efforts have resulted in the emergence of fluorescence-mediated tomography (FMT) as a technique for quantitative *in vivo* molecular imaging using fluorescent agents.

Phantom experiments using known fluorochrome concentrations have demonstrated the accuracy of FMT employing a normalized Born reconstruction strategy in measuring fluorochrome concentrations in homogeneous media.^{34,38} However, it has not been established that the quantitative performance of fluorescence tomography observed *in vitro* extends to the *in vivo* situation. This validation includes not only evaluation of the quantitative accuracy of FMT for fluorescent objects in living subjects, but also determining how factors such as background fluorescence and local optical properties affect this accuracy. These questions are directly applicable to biological situations involving quantitation of a fluorescent target, such as a tumor that has been labeled through accumulation and/or activation of a fluorescent probe. In such an experiment, one wishes to absolutely determine the fluorochrome concentration and hence probe accumulation/activation within the tumor. This measurement should ideally be independent of low levels of background fluorescence in surrounding tissue as well as the optical properties of the tumor itself, which are in part determined by its blood content and vascularity.

The extent to which FMT satisfies these criteria was investigated in this study by imaging tumor-like phantoms containing known concentrations of fluorescent dye before and after subcutaneous implantation in nude mice. Comparisons were made between reconstructions of FMT data acquired before and after implantation of the fluorescent tubes, allowing estimation of the sensitivity of FMT to the optical heterogeneity of the surrounding mouse tissues. In addition, identical tubes were imaged in mice after intravenous injection of a fluorescent probe targeting phosphatidylserine, a cell surface moiety implicated in cellular apoptosis. The selection of this probe represents a realistic case of a nonactivatable probe that typically yields background fluorescence signals due to nonspecific biodistribution. This case allowed observation of the effects of background, nonspecific fluorescence on the quantitation of a fluorescent focus. Finally, the influence of local optical heterogeneities on quantitation accuracy were assessed by imaging implanted fluorescent tubes with varying ink concentrations. From these experiments, it was observed that large dataset fluorescence tomography using a normalized Born reconstruction methodology can offer reliable quantification performance *in vivo*.

2 Methods and Materials

2.1 Fluorescent Tube Construction and Implantation

A turbid fluorescent medium simulating fluorochromes embedded in tissue was created by adding Cy 5.5 fluorescent dye (peak excitation 670 nm, peak emission 710 nm) to a solution of 1% intralipid and black india ink. The exact concentrations of Cy 5.5 and ink varied based on the experiment and are described in detail later. Translucent plastic tubes of inner diameter 1.5, wall thickness 0.25 mm, and length 8 mm, as shown in Fig. 1, were sealed at one end and filled with 6 μL of the fluorescent medium. The end of the tube was then sealed by melting the plastic at the opening. All animals were

treated in accordance with the regulations of Massachusetts General Hospital. Nude mice (nu/nu, COX-7) were prepared for fluorescent tube placement by administration of general anesthesia through an intraperitoneal injection of ketamine (80 mg/kg) and xylazine (12 mg/kg). A 5-mm incision was made in the skin at the superior aspect of the ventral mammary fat pad, and a subcutaneous pocket approximately 10 mm long was made by separating the skin from the underlying muscle. A fluorescent tube was completely inserted into the subcutaneous pocket, after which the mouse was imaged with the system and protocol discussed in the next section. The tube was then removed and the implantation and imaging procedure was repeated using a new tube, depending on the experiment as detailed next. A single dose of anesthesia for a mouse was sufficient for fluorescent tube implantation and the acquisition of all subsequent data. After completion of the imaging battery and while still under anesthesia, the mice were euthanized by an overdose of halothane.

2.2 Data Acquisition and Analysis

A CCD-based parallel-plate imaging chamber designed for fluorescence reflectance and tomographic imaging of mice was used for all imaging experiments in this study.³⁴ A diagram of the imaging chamber setup is shown in Fig. 1. After positioning each subject within the chamber and adjusting the plates to a separation of 13 mm, an imaging examination consisting of four image sets was acquired. Initially, an image of the subject was obtained under white light illumination to determine the position of the target and extract the location of each of the tomographic sources. A diode laser of wavelength 670 nm was then used to illuminate the subject in a reflectance geometry, and an FRI image was acquired by placing a four-cavity bandpass filter centered at 710 nm and a longpass filter with a cutoff wavelength of 695 nm in front of the CCD camera. The subject was then immersed in a 1% intralipid and 50 ppm black india ink solution ($\mu_a=0.3 \text{ cm}^{-1}$, $\mu'_s=8.0 \text{ cm}^{-1}$), designed to match the bulk optical properties of mice,³⁹ for acquisition of the tomographic data. Images of the photon distribution at the fluorescent excitation wavelength at the detector window were acquired for each of the 32 tomographic sources, spanning a field of view of 18×12 mm, using a four-cavity bandpass filter centered at 670 nm and a 1.5 optical density neutral density filter. The corresponding images at the fluorescent emission wavelength were then obtained using the same filter set as was employed for FRI. These images comprise a set of transillumination measurements at the fluorescent excitation and emission wavelengths, and constitute the raw dataset used for subsequent tomographic reconstruction.

After resampling the excitation and emission images to detector grids of 19×13 over a 18×12 -mm field of view and correcting for the effects of the filter sets used, these data were reconstructed using a computationally efficient normalized Born approach employing a homogeneous slab solution to the diffusion equation.²⁸ Briefly, the normalized Born field was calculated by dividing the emission images, corrected for filter bleedthrough of excitation light, by the excitation images. Fluorescence measurements less than ten standard deviations above the noise level of the emission acquisitions were ignored. This measurement, deemed U^{mB} , can be related

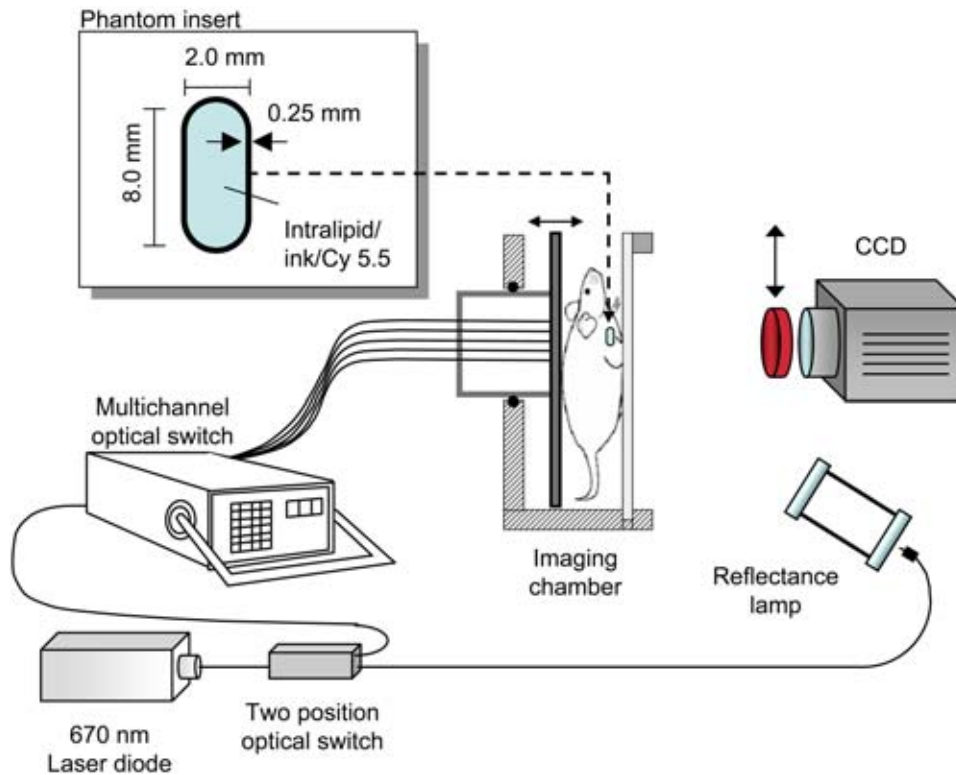


Fig. 1 The experimental setup used for the *in vivo* measurements. A small plastic tube filled with a turbid intralipid/ink/Cy 5.5 solution is implanted in a nude mouse, which is then placed in an imaging chamber and bathed in an intralipid and ink optical matching fluid. A 670-nm wavelength laser diode, suitable for the excitation of Cy 5.5 fluorescent dye, is routed into a two-channel optical switch. Light is then routed either into a lamp adjacent to the detection apparatus, facilitating FRI, or into a multichannel optical switch that controls the excitation sources used for FMT. Photon detection is accomplished with a CCD camera focused on a window implanted in the imaging chamber. Appropriate bandpass filters are used to selectively detect fluorescent excitation or emission photons.

to the spatial fluorochrome concentration distribution $n(\mathbf{r})$ by the expression

$$U^{nB}(\mathbf{r}_s, \mathbf{r}_d) = \frac{S_0}{U(\mathbf{r}_s, \mathbf{r}_d)} \cdot \int \left(U(\mathbf{r}_s, \mathbf{r}) \cdot \frac{n(\mathbf{r})v}{D} \cdot G(\mathbf{r}_d - \mathbf{r}) \right) d^3r, \quad (1)$$

where $U(\mathbf{r}_s, \mathbf{r})$ is the photon field at the excitation wavelength λ_1 induced at position \mathbf{r} by a source at position \mathbf{r}_s , and $G(\mathbf{r}_d - \mathbf{r})$ is the Green's function describing photon propagation at the emission wavelength λ_2 from a point \mathbf{r} to a detector at location \mathbf{r}_d . For this experimental setup, a Green's function describing photon propagation through a slab was used to model light passing through the rectangular chamber enclosing the subject, filled with an intralipid-ink matching fluid. D is the diffuse medium diffusion coefficient, v is the speed of light in the medium, and S_0 is an experimentally determined calibration factor that collectively accounts for the laser power and the unknown gain and attenuation factors of the system. This expression was discretized and inverted to solve for $n(\mathbf{r})$ using 20 iterations of an arithmetic reconstruction technique inversion procedure using randomly ordered projections.⁴⁰ The initial voxel estimates for $n(\mathbf{r})$ were set to zero.

The result of the reconstruction was a 3-D grid with $28 \times 20 \times 18$ elements over a $20 \times 14 \times 12$ -mm field of view

representing the fluorochrome concentration in the chamber. This field of view was chosen as it allowed the acquisition of a high resolution dataset over a volume that included both the target as well as surrounding anatomy. Reconstructions were performed on a Pentium 4 PC with a processor clock speed of 2.4 GHz and 1 gigabyte of RAM (Dell, Austin, Texas). The mean intensity of the reconstructed fluorescent tube was calculated by averaging the intensity of voxels in a five by five neighborhood from the slice in the reconstructed volume corresponding to the location of the tube. The neighborhood was centered on the voxel with the maximum voxel intensity in the slice. The correspondence between the location of these voxels and the location of the fluorescent tube was verified visually through comparison with the white light and fluorescent reflectance images. Artifacts encountered in voxels near the sources and detectors, because of the large weights associated with them in the forward model, were avoided by excluding slices at the edges of the reconstructed volume from the analysis. For these experiments, this was not a significant concern, as the target was positioned outside these locations.

2.3 Influence of Biological Optical Heterogeneity

Fluorescent tubes with Cy 5.5 concentrations of 0, 250, 500, and 1000 nM (0, 1.5, 3, and 6 picomoles Cy 5.5 in 6 μ L of solution) and an ink concentration of 50 ppm were constructed. The tubes were first sequentially implanted in a nude

mouse and imaged with the FRI/FMT system, generating data hereafter referred to as the *in vivo* measurements. The fluorescent tubes were then removed from the mouse and sequentially imaged again while suspended in the 1% intralipid, 50-ppm ink optical matching fluid, positioned just behind the glass window as they were while in the subcutaneous space. These data are hereafter referred to as the *ex vivo* measurements. Reconstructions of the *in vivo* and *ex vivo* measurements were compared to assess the effect of the heterogeneous optical medium of the mouse on the ability of FMT to resolve fluorochrome concentrations. This experiment was repeated three times to obtain an estimate of the variability of the findings.

2.4 Influence of Background Fluorescence

To observe the effects of low levels of distributed background fluorescence on the quantitation of a fluorescent target, a nude mouse was injected with 1.0 nM of Cy 5.5-labeled Annexin V, a fluorescent probe with affinity for apoptotic cells exhibiting phosphatidylserine on the outer leaflet of the cell membrane.³ Because this probe is nonactivatable (i.e., constitutively fluorescent), it produces detectable levels of fluorescence in nonapoptotic tissues because of nonspecific distribution by the vascular system. Given typical mouse body masses and volumes and the biodistribution of Annexin V, we estimate that this will result in a background Cy 5.5 concentration of approximately 50 nM. After allowing the probe to circulate for 1.5 h, tubes with Cy 5.5 concentrations of 0, 250, 500, and 1000 nM (0, 1.5, 3, and 6 picomoles Cy 5.5 in 6 μ L of solution) and an ink concentration of 50 ppm were consecutively implanted subcutaneously and imaged with FRI and FMT. This model therefore simulates a fluorescent tumor in the presence of a background of distributed, nonspecific fluorescence. The tubes were then removed from the Cy 5.5 Annexin V injected mouse and imaged again after implantation into a nude mouse that had not been injected with the probe.

FMT datasets were reconstructed using a single calibration factor S_0 determined from the *in vivo* fluorescent tube experiments in the previous section. Comparisons between measurements made with and without a circulating probe demonstrated the effects of background signals on FMT reconstructions. As previously stated, the experiment was repeated three times. We further investigated whether a simple offset subtraction could correct for the influence of background fluorochromes on the quantitation of a fluorescent focus. To accomplish this, the data acquired from mice injected with Cy 5.5 Annexin V were reconstructed a second time after subtracting a value of 20 counts/s from every measurement of the fluorescence field. The offset of 20 counts/s was determined by calculating the counts over a region of interest distant from the fluorescent tube in the fluorescent measurements taken from multiple mice injected with the Annexin V Cy 5.5 probe.

2.5 Influence of Target Absorption

Fluorescent tubes with ink concentrations of 25, 50, and 100 ppm and a Cy 5.5 concentration of 500 nM (3 picomoles Cy 5.5 in 6 μ L of solution) were constructed to simulate tumors with the same level of fluorescence but different absorption coefficients, corresponding to the biological situation

of tumors with different degrees of vascularity and hence blood-related photon absorption. These tubes were sequentially implanted subcutaneously and imaged with FRI and FMT. Reconstructions of the FMT, calibrated using a factor determined from the *in vivo* measurements in the first section, were inspected to determine the effects of local optical properties within the imaging target on the fluorochrome concentrations measured by FMT. As before, the experiment was repeated three times.

3 Results

A total of 39 FRI/FMT datasets were acquired from six nude mice over the course of the experiments described. A single FRI/FMT examination, including insertion of the fluorescent tube, positioning of the mouse within the imaging chamber, and acquisition of a single FRI and FMT dataset, required approximately 10 min. Reconstruction of raw FMT data into a 3-D fluorochrome distribution was completed in approximately 5 min per dataset.

3.1 Influence of Biological Optical Heterogeneity

Figure 2(a) shows a representative reconstructed FMT dataset as a series of coronal slices, parallel to the source and detector planes. Reconstructed FMT slices acquired from a fluorescent tube containing 1000 nM Cy 5.5, imaged first by itself and then again after subcutaneous implantation in the mammary fat pad of a nude mouse, are shown overlaid on corresponding white light images in Figs. 2(b) and 2(c). In these overlays, FMT pixels with values less than the minimum of the colorbar were made transparent so as to visualize the location of the FMT focus relative to the white light image. The FMT slices represented are 0.6 mm-thick sections located 1.6 mm behind the glass observation window of the chamber, which is the expected position of the tube given its placement. In both measurements, the tube reconstructs as a fluorescent cylinder with dimensions of approximately 3 by 1.5 mm, as determined by full width at half maximum, which correlates with the volume and dimensions of the fluorochrome solution within the plastic tube (6 μ L, 3.3 mm long, with a 1.5 mm diameter). The quantitated fluorochrome concentrations from each situation are within 10% of each other, with the values in the *in vivo* case being slightly elevated relative to the *ex vivo* case.

The average fluorochrome concentrations for tubes with Cy 5.5 concentrations of 0, 250, 500, and 1000 nM imaged *in vivo* and *ex vivo* are plotted in Fig. 2(d). For each concentration, the FMT measurement acquired with the fluorescent tube implanted subcutaneously (triangles) reconstructed to fluorochrome concentrations 10 to 20% larger than the corresponding measurement acquired with the tube immersed in intralipid (circles). Both the *in vivo* and *ex vivo* measured fluorochrome concentrations are within 5 to 10% of the actual fluorochrome concentration, as identified by the dotted line. These data were used to calculate a single calibration factor S_0 to account for the unknown laser strength and CCD gain, and convert reconstructed values to absolute fluorochrome concentrations. This calibration factor is used in all subsequent measurements.

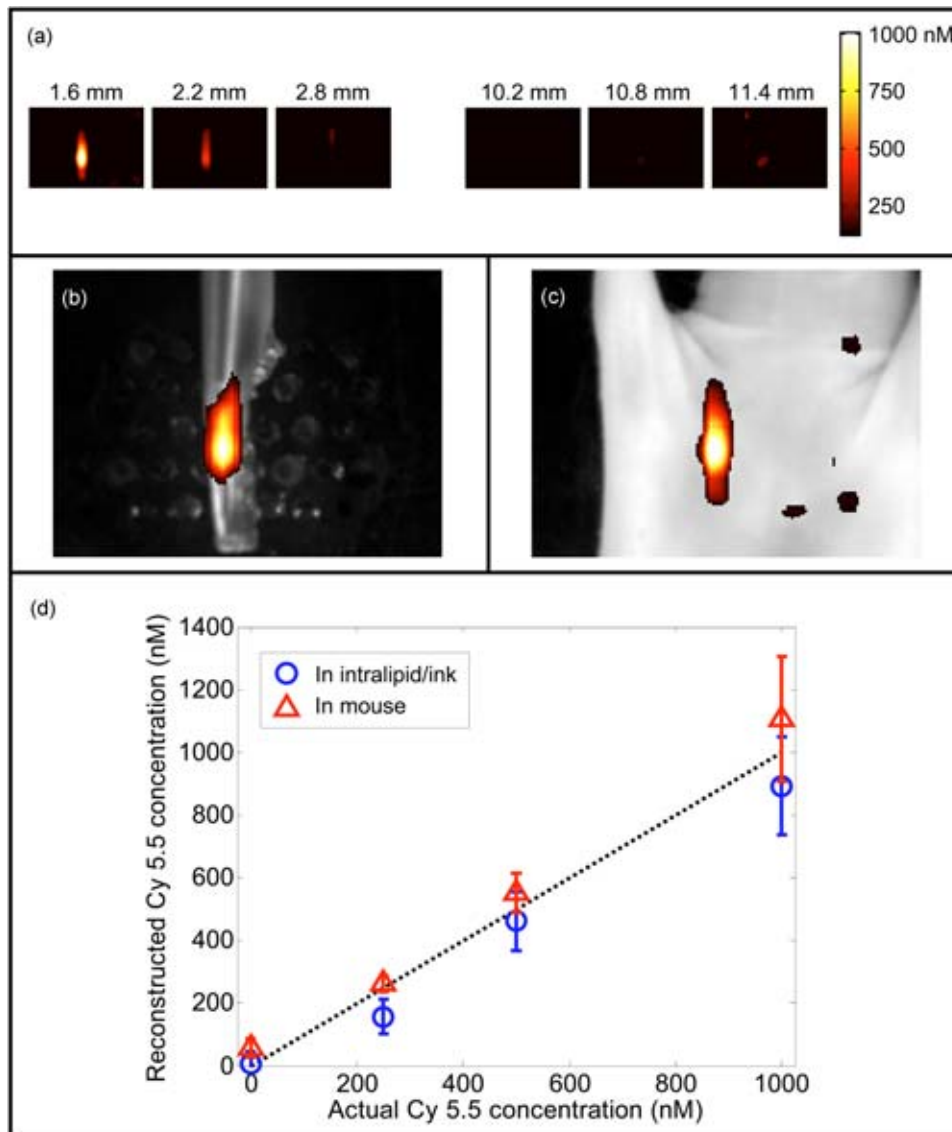


Fig. 2 FMT of fluorescent tubes before and after subcutaneous implantation in a nude mouse. (a) A series of coronal slices from a reconstructed FMT dataset acquired from a fluorescent tube containing 1000-nM Cy 5.5 implanted subcutaneously in a nude mouse. Slice locations are given as distances from the glass imaging window, with the source plane being at a depth of 13 mm. The central slices contained no significant signals and are omitted. The scale bar in (a) applies to (b) and (c). (b) A 1.6-mm-deep reconstructed FMT slice acquired from a fluorescent tube containing 1000-nM Cy 5.5 immersed in an intralipid and ink solution. The FMT slice is shown overlaid on a white light image of the tube. (c) A corresponding reconstructed FMT overlay from a dataset acquired after implanting the same fluorescent tube subcutaneously in a nude mouse. (d) Average fluorochrome concentrations measured from fluorescent tubes containing 0-, 250-, 500-, and 1000-nM Cy 5.5 plotted against actual fluorochrome concentration. Measurements obtained with the tube immersed in a homogeneous medium are represented as circles, while measurements made after implantation of the tube in a living subject are shown as triangles. Error bars represent the standard deviation of three independent measurements.

3.2 Influence of Background Fluorescence

A slice from the FMT reconstruction of a 500 nM fluorescent tube implanted in mice preinjected with Cy 5.5-labeled Annexin V are shown in Fig. 3(b), while a corresponding FMT slice acquired from a mouse that was not injected with a probe is shown in Fig. 3(a). The slices were taken from the same locations as those presented in Figs. 2(b) and 2(c). The reconstructed volumes in these images have dimensions of 2.5 by 2 mm, and are more spherical than those obtained with the 1000 nM phantom in Fig. 2. It is immediately apparent that in addition to the fluorescent tube, background heterogeneities

are present in the reconstructions of data for which the mouse was initially injected with a fluorescent agent. The effects of these heterogeneities on quantitation of the fluorescent tubes are shown graphically in Fig. 3(d), in which average fluorochrome concentrations measured by FMT are plotted as a function of the tube Cy 5.5 concentration. The trace representing acquisitions made in a mouse with no circulating probe (circles) closely follows the actual fluorochrome concentrations, shown as a dotted line. The reconstructions of data acquired from a mouse injected with Cy 5.5-labeled Annexin V (squares), however, demonstrate a pronounced deviation from

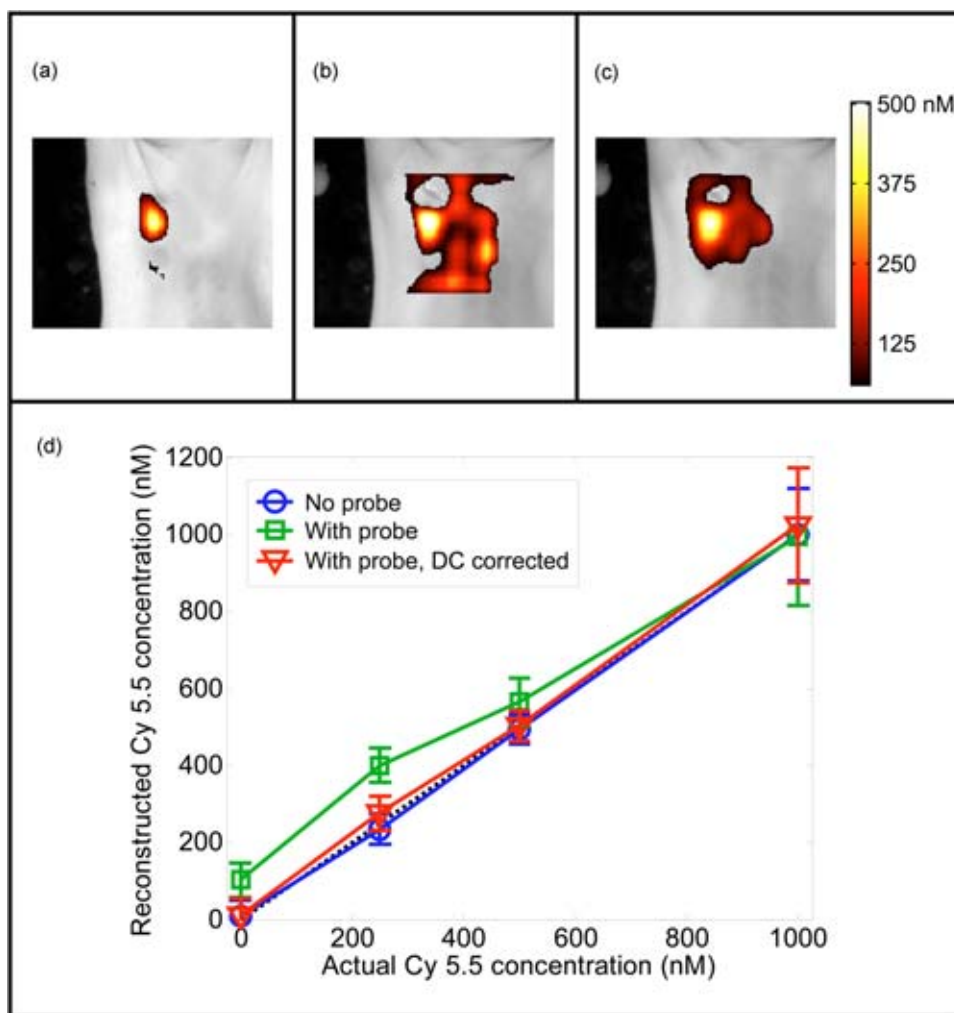


Fig. 3 FMT of fluorescent tubes in nude mice with and without previous intravenous injection of Cy 5.5-labeled Annexin V. (a) A 1.6-mm-deep coronal reconstructed FMT slice of a fluorescent tube containing 500-nM Cy 5.5 subcutaneously implanted in a mouse with no injected fluorescent probe, shown overlaid on the corresponding white light image. (b) A corresponding reconstructed FMT slice acquired from 500-nM Cy 5.5 phantom subcutaneously implanted in a mouse injected with 2 nM of Annexin V Cy 5.5 1.5 h before imaging. (c) An FMT slice reconstructed from the raw data in (b) after applying a correction for background fluorescence. The scale bar shown applies to (a), (b), and (c). (d) Fluorochrome concentrations measured from FMT reconstructions of fluorescent tubes in mice with and without background fluorescence and with and without background correction plotted as a function of the actual tube fluorochrome concentrations. Error bars represent the standard deviation of three independent measurements.

the actual values at lower tube fluorochrome concentrations (0 to 500 nM). For the 1000 nM fluorescent tube experiment, the traces for the two acquisitions converge.

A simple correction for background fluorescence was applied by subtracting 20 counts/s from all fluorescence measurements prior to solving the inverse problem. Fluorochrome concentrations reconstructed from these corrected FMT datasets are shown in the red trace in Fig. 3(d). The result of the correction is that reconstructed FMT fluorochrome concentrations approach those obtained from the same fluorescent tubes imaged in mice without background fluorescence. The effect of this correction on the reconstructed image is shown in Fig. 3(c), which shows the FMT slice from Fig. 3(b) reconstructed after dc subtraction. The background heterogeneities in the image are reduced, and the reconstructed fluorochrome concentrations in the focus approach the values measured

from the fluorescent tube in a mouse with no background fluorescence.

3.3 Influence of Target Absorption

The effect of varying local absorption on FMT measurements was assessed by imaging fluorescent tubes containing 500 nM Cy 5.5 and 25, 50, or 100 ppm black india ink, as shown in Figs. 4(a)–4(c). The reconstructed volumes in these images have dimensions 2.5 by 2 mm, and appear similar in shape to those observed in Fig. 3. As depicted in the bar graph in Fig. 4(d), the average reconstructed FMT fluorochrome concentrations are approximately equal for the tubes containing 25 and 50 ppm ink, while the average fluorochrome concentration for the tube containing 100-ppm ink was approximately 20% larger. This difference is on the order of the

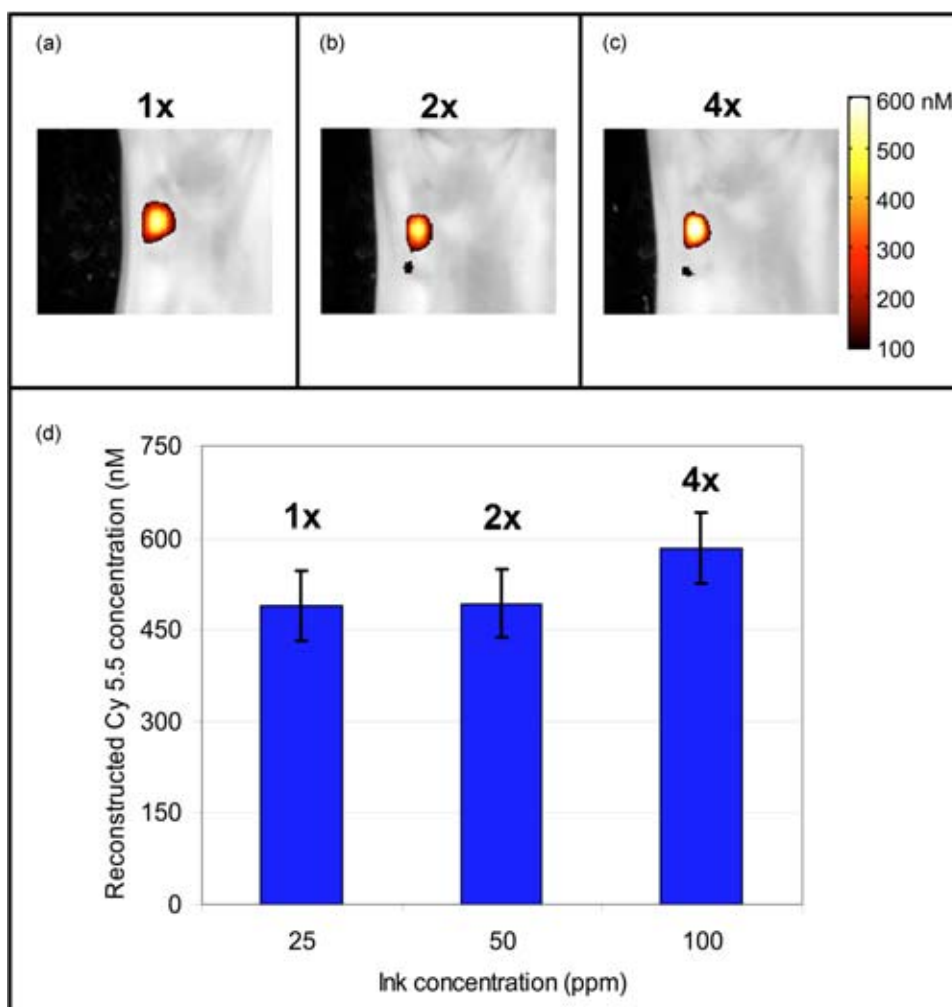


Fig. 4 FMT of fluorescent tubes with varying ink concentrations in nude mice. Coronal slices located 1.6 mm beneath the imaging window taken from FMT reconstructions of fluorescent tubes containing 500-nM Cy 5.5 and (a) 25-, (b) 50-, and (c) 100-ppm ink implanted in a nude mouse overlaid on white light images, with a scale bar that applies to each image. (d) A bar graph of the reconstructed fluorochrome concentration versus the actual concentration, with error bars representing the standard deviation of three independent measurements.

measurement variability, as given by the error bars in Fig. 4(d). In contrast, a 40% decrease in photon counts was measured between FRI images collected from the fluorescent tubes containing 25 and 100 ppm ink.

4 Discussion

The quantitative accuracy of fluorescence tomography has been investigated previously.^{32,34} However, these studies involved titrations of known amounts of fluorescent dye into a translucent tube immersed in a turbid solution of intralipid and ink. This idealized experiment utilizing a homogeneous medium may not reflect the performance of FMT *in vivo*, where biological optical heterogeneity and background fluorescence may complicate the measurement of fluorochrome concentrations. In the present study, we sought to generate a model system in which we could probe the quantitative performance of FMT in living subjects. By creating small clear plastic vessels that were filled with known concentrations of fluorescent dye, we were able to produce a controlled phantom that could be inserted subcutaneously to mimic a subcu-

taneous tumor model containing a known amount of fluorochrome. Furthermore, by adding intralipid and ink to the fluorochrome solution in the tube, we simulated the biological situation of fluorochromes embedded in a turbid, absorbing tissue. This experimental system allowed the evaluation of the response of FMT to biological heterogeneity, background fluorescence, and local tissue absorption.

FMT reconstructions of measurements taken of the same fluorescent tube both before and after implantation in a nude mouse demonstrate a linear relationship between measured and actual fluorochrome concentration. FMT reconstructions of fluorescent tubes imaged while in a mouse were observed to give larger fluorochrome concentration measurements than when the tubes are imaged in a homogeneous intralipid-ink medium, as seen in Fig. 2. The slope of the regression between measured and actual fluorochrome concentrations in the *in vivo* case was 24.7% greater than that in the *ex vivo* case. This effect can be attributed to the optical heterogeneity of the animal that typically yields a higher net absorption coefficient for photon paths passing through the middle of the

torso, because of the heat and other highly absorbing structures, relative to photon paths through boundaries that generally contain low-absorbing adipose tissue. This quantification bias in the presence of increased absorption was also observed in the results of Fig. 4, and is discussed further below. This discrepancy could be addressed by incorporating independent reconstructions of background absorption, yielding more accurate forward models for fluorescence tomography. An alternative approach is to employ an experiment-based calibration factor derived from animal measurements to improve *in vivo* quantification. It is important to note that, similar to observations obtained in simpler phantoms, normalized Born methods yield robust reconstruction of subcutaneous fluorescent foci even in the presence of biological heterogeneity.

One of the most exciting possibilities for fluorescence tomography is its application in the detection of molecular-specific fluorescent probes *in vivo*, permitting noninvasive visualization of a range of biochemical and physiologic activity. In these applications, the sensitivity of FMT to background fluorescence due to nonspecific probe accumulation in tissues within the field of view becomes critical. In this study, we have addressed this issue by injecting mice with implanted subcutaneous fluorescent tubes with a standard dose of a representative fluorescent molecular probe, Cy 5.5 Annexin V. As the animal model does not contain a focus of apoptotic activity in which accumulation of this probe might be expected, the agent follows its normal biodistribution, resulting in distributed, diffuse fluorescent signals throughout the subject. As observed in Figs. 3(a) and 3(b), FMT measurements of this model to identify the presence of the subcutaneous fluorescent tube. However, there are also low levels of fluorochrome reconstructed in the background, which are not observed in reconstructions of measurements in which the mouse was not injected with a probe. Background fluorescence clearly affects measurement of focal fluorochrome concentrations in a structure of interest, as evidenced by Fig. 3(b), where a 500 nM target was measured to have a fluorochrome concentration of 600 nM. With increased target fluorochrome concentration, the effect of background fluorescence becomes less noticeable, as observed in Fig. 3(d).

To advance FMT as an imaging modality capable of quantitatively measuring fluorochrome concentrations in heterogeneous, *in vivo* settings, the influence of background fluorescence on imaging results must be addressed. As a preliminary approach, we applied a correction in which a dc value of 20 counts/s was subtracted from all fluorescence field measurements prior to image reconstruction. This procedure makes the approximation that the contribution of the background fluorochrome distribution adds 20 counts/s for each source-detector pair. While this correction proved to be quite effective in this study for generating measurements that are unaffected by background fluorescence, as seen in Fig. 3(d), it is not a robust means of dealing with background signals. Further work is being conducted to develop adaptive techniques for measuring background fluorescence and subtracting its contribution to the measured fluorescence photon field. Effort is also being directed to develop more sophisticated treatments of photon propagation from small concentrations of distributed fluorochromes, and to develop to more accurately correct for the effects of a background of low intensity fluorescence in *in vivo* FMT datasets.

As discussed before, tomographic measurements of fluorescence can be greatly influenced by the optical properties of the surrounding medium. However, for measurements of tumors and tumor models targeted by fluorescent contrast agents, the local optical properties of the fluorescent object itself can also be of significance. Different tumor types can exhibit a wide variety of vascular profiles and therefore blood contents. As hemoglobin is a strong photon absorber in the near-infrared band, this can result in different tumors possessing distinct photon absorption properties. We simulated this phenomenon by constructing fluorescent tubes with varying concentrations of black india ink mixed with the intralipid and Cy 5.5 solution. Spectrophotometer measurements verified that the corresponding absorption coefficients of the resulting solutions ranged from 0.15 cm^{-1} (25 ppm ink) to 0.6 cm^{-1} (100 ppm ink). As seen in Fig. 4(d), our data suggest that the effect of varying local absorption on fluorochrome concentrations measured by FMT is limited. Tubes with ink concentrations of 25 and 50 ppm ($\mu_a=0.15$ and 0.3 cm^{-1}) reconstructed to average fluorochrome concentrations of 489 and 492 nM, respectively, while a tube with 100-ppm ink ($\mu_a=0.6 \text{ cm}^{-1}$) reconstructed to an average fluorochrome concentration of 582 nM. It is encouraging that given a four-fold change in the absorption coefficient of the fluorescent tube, the fluorochrome concentration measured by FMT changed only by approximately 20%. Corrections involving measured or *a priori* information on absorption heterogeneities in the subject may further reduce this variation and maximize the accuracy of quantitation for FMT. FRI, however, is unable to distinguish changes in absorption from changes in fluorochrome concentrations in the target, as evident by the 40% decrease in photon counts measured from the phantoms with absorption coefficients of 0.15 and 0.6 cm^{-1} . This benefit of FMT relative to FRI has recently been demonstrated by Ntzachristos et al. by imaging tumors with different degrees of vascularity.²¹

The results shown herein were obtained with a second-generation FMT prototype employing 31 light sources and an array of 19×13 detectors sampled from the CCD images acquired. These data were reconstructed using a homogeneous slab solution to the diffusion equation after the normalized Born formulation. This approach demonstrated reduced sensitivity on varying medium optical properties and is experimentally simple to implement, as it is independent of the source and detector gain and several coupling issues between tissue and the optical apparatus. Current research in acquisition hardware and reconstruction techniques for FMT can be expected to further refine the quantitative accuracy of fluorescence tomography *in vivo*. In particular, optimization studies are shedding light on the source and detector arrays that most effectively balance dataset size and information content for small animal imaging.^{41,42} Also, progress has been made toward more accurately modeling the photon propagation boundaries encountered in FMT,^{36,43} permitting fluorescence tomography without the assumption of a slab geometry, and therefore without bathing the subject in an optical matching fluid. Other groups have also had success in combining high resolution anatomic imaging techniques such as magnetic resonance imaging (MRI) with diffuse optical tomography, permitting consideration of tissue optical heterogeneity in the

tomographic reconstruction process.⁴⁴ Finally, in contrast to the diffusion equation-based solutions used herein, the use of forward models based on the transport equation may be used to improve the fluorescence imaging problem,⁴⁵ especially in systems with small source-detector separations (less than 5 to 10 photon mean-free paths) and when imaging through void regions. More advanced theoretical approaches to the problem of photon propagation in tissue can improve the imaging accuracy, especially when imaging absolute quantities. These developments can further improve FMT robustness and image fidelity, and can be used to specifically detect and measure fluorescence in live tissues.

5 Conclusion

We demonstrate the ability of a fluorescent molecular tomography system to measure fluorochrome concentrations *in vivo*. Furthermore, we show that the quantitative accuracy of FMT is robust in the presence of varying local photon absorption coefficients. The presence of background fluorescence, modeled here by a previous intravenous injection of a fluorescent-labeled molecular probe in a mouse bearing a fluorescent tube, is seen to offset fluorochrome concentrations measured by FMT for tubes with Cy 5.5 concentrations from 0 to 500 nM Cy 5.5. This effect is reduced by applying a simple correction for background fluorescence to the measured fluorescent field. Advances in FMT hardware and software will further reduce the sensitivity of the technique to background fluorescence and to local absorption. These findings encourage the use of fluorescence tomography as a quantitative technique for measuring molecular-specific fluorescent probes *in vivo*, supporting the development of this emerging branch of molecular imaging.

Acknowledgments

The authors gratefully acknowledge the contributions of Ralf Schulz, Anabela da Silva, Giannis Zacharakis, and Andreas Yulliano to this work. This work was supported in part by the National Institute of Health grants P50 CA 86355, R24 CA 92782, RO1 EB 000750-1, R21 CA 91807, and T32 CA 79443.

References

1. S. Folli, P. Westermann, D. Braichotte, A. Pelegrin, G. Wagnières, H. Van den Berg, and J. P. Mach, "Antibody-indocyanin conjugates for immunophotodetection of human squamous cell carcinoma in nude mice," *Cancer Res.* **54**, 2643–2649 (1994).
2. D. Neri, B. Carnemolla, A. Nissim, A. Leprini, G. Querzè, E. Balza, A. Pini, L. Tarli, C. Halin, P. Neri, L. Zardi, and G. Winter, "Targeting by affinity-matured recombinant antibody fragments of an angiogenesis associated fibronectin isoform," *Nat. Biotechnol.* **15**, 1271–1275 (1997).
3. E. Schellenberger, A. Bogdanov, A. Petrovsky, V. Ntziachristos, R. Weissleder, and L. Josephson, "Optical imaging of apoptosis as a biomarker of tumor response to chemotherapy," *Neoplasia* **5**, 187–192 (2003).
4. S. Achilefu, R. B. Dorshow, J. E. Bugaj, and R. Rajagopalan, "Novel receptor-targeted fluorescent contrast agents for *in vivo* tumor imaging," *Invest. Radiol.* **35**, 479–485 (2000).
5. A. Becker, C. Hennenius, K. Licha, B. Ebert, U. Sukowski, W. Semmler, B. Wiedenmann, and C. Grotzinger, "Receptor-targeted optical imaging of tumors with near-infrared fluorescent ligands," *Nat. Biotechnol.* **19**, 327–331 (2001).
6. R. Weissleder, C. H. Tung, U. Mahmood, and A. Bogdanov, "In vivo imaging of tumors with protease-activated near-infrared fluorescent probes," *Nat. Biotechnol.* **17**, 375–378 (1999).
7. S. Tyagi and F. R. Kramer, "Molecular beacons: probes that fluoresce upon hybridization," *Nat. Biotechnol.* **14**, 303–8 (1996).
8. M. Yang, E. Baranov, P. Jiang, F. Sun, L. Li, S. Hasegawa, M. Bouvet, M. Al-Tuwaijri, T. Chishima, H. Shimada, A. R. Moossa, S. Penman, and R. M. Hoffman, "Whole-body optical imaging of green fluorescent protein-expressing tumors and metastases," *Proc. Natl. Acad. Sci. U.S.A.* **97**, 1206–1211 (2000).
9. M. Rajadhyaksha, M. Grossman, D. Esterowitz, R. H. Webb, and R. R. Anderson, "In vivo confocal laser microscopy of human skin: melanin provides strong contrast," *J. Invest. Dermatol.* **104**, 946–952 (1995).
10. B. R. Masters, P. T. C. So, and E. Gratton, "Multiphoton excitation fluorescence microscopy and spectroscopy of *in vivo* human skin," *Biophys. J.* **72**, 2405–2412 (1997).
11. S. Gonzalez, M. Rajadhyaksha, G. Rubinstein, and R. R. Anderson, "Characterization of psoriasis *in vivo* by reflectance confocal microscopy," *J. Med.* **30**, 337–356 (1999).
12. P. T. C. So, C. Y. Dong, B. R. Masters, and K. M. Berland, "Two-photon excitation fluorescence microscopy," *Annu. Rev. Biomed. Eng.* **2**, 399–429 (2000).
13. W. L. Monsky, D. Fukumura, T. Gohongi, M. Ancukiewicz, H. A. Weich, V. P. Torchilin, F. Yuan, and R. K. Jain, "Augmentation of transvascular transport of macromolecules and nanoparticles in tumors using vascular endothelial growth factor," *Cancer Res.* **59**, 4129–4135 (1999).
14. M. Dellian, F. Yuan, V. S. Trubetskoy, V. P. Torchilin, and R. K. Jain, "Vascular permeability in a human tumour xenograft: molecular charge dependence," *Br. J. Cancer* **82**, 1513–1518 (2000).
15. U. Mahmood, C. H. Tung, A. Bogdanov, and R. Weissleder, "Near infrared optical imaging system to detect tumor protease activity," *Radiology* **213**, 866–870 (1999).
16. J. S. Reynolds, T. L. Troy, R. H. Mayer, A. B. Thompson, D. J. Waters, K. K. Cornell, P. W. Snyder, and E. M. Sevick-Muraca, "Imaging of spontaneous canine mammary tumors using fluorescent contrast agents," *Photochem. Photobiol.* **70**, 87–94 (1999).
17. A. Zaheer, R. E. Lenkinski, A. Mahmood, A. G. Jones, L. C. Cantley, and J. V. Frangioni, "In vivo near-infrared fluorescence imaging of osteoblastic activity," *Nat. Biotechnol.* **19**, 1148–1154 (2001).
18. J. E. Bugaj, S. Achilefu, R. B. Dorshow, and R. Rajagopalan, "Novel fluorescent contrast agents for optical imaging of *in vivo* tumors based on a receptor-targeted dye-peptide conjugate platform," *J. Biomed. Opt.* **6**, 122–133 (2001).
19. V. Ntziachristos, C. Bremer, and R. Weissleder, "Fluorescence imaging with near-infrared light: new technological advances that enable *in vivo* molecular imaging," *Eur. Radiol.* **13**, 195–208 (2003).
20. B. W. Pogue, S. L. Gibbs, B. Chen, and M. Savellano, "Fluorescence imaging *in vivo*: Raster scanned point-source imaging provides more accurate quantification than broad beam geometries," *Technol. Cancer Res. Treat.* **3**, 15–21 (2004).
21. V. Ntziachristos, E. A. Schellenberger, J. Ripoll, D. Yessayan, E. Graves, A. Bogdanov, L. Josephson, and R. Weissleder, "Visualization of antitumor treatment by means of fluorescence molecular tomography with an annexin V-Cy 5.5 conjugate," *Proc. Natl. Acad. Sci. U.S.A.* **101**, 12294–12299 (2004).
22. E. L. Hull, M. G. Nichols, and T. H. Foster, "Localization of luminescent inhomogeneities in turbid media with spatially resolved measurements of cw diffuse luminescence emittance," *Appl. Opt.* **37**, 2755–2765 (1998).
23. V. Chenomordik, D. Hattery, I. Gannot, and A. H. Gandjbakhche, "Inverse method 3-D reconstruction of localized *in vivo* fluorescence—application to Sjogren syndrome," *IEEE J. Sel. Top. Quantum Electron.* **54**, 930–935 (1999).
24. J. H. Chang, H. L. Graber, and R. L. Barbour, "Imaging of fluorescence in highly scattering media," *IEEE Trans. Biomed. Eng.* **44**, 810–822 (1997).
25. J. Wu, L. Perelman, R. R. Dasari, and M. S. Feld, "Fluorescence tomographic imaging in turbid media using early-arriving photons and Laplace transforms," *Proc. Natl. Acad. Sci. U.S.A.* **94**, 8783–8788 (1997).
26. H. Jiang, "Frequency-domain fluorescent diffusion tomography: a finite-element-based algorithm and simulations," *Appl. Opt.* **37**, 5337–5343 (1998).
27. R. Roy and E. M. Sevick-Muraca, "Three-dimensional unconstrained and constrained image-reconstruction techniques applied to fluores-

- cence, frequency-domain photon migration," *Appl. Opt.* **40**, 2206–2215 (2001).
28. V. Ntziachristos and R. Weissleder, "Experimental three-dimensional fluorescence reconstruction of diffuse media using a normalized Born approximation," *Opt. Lett.* **26**, 893–895 (2001).
 29. M. J. Eppstein, D. J. Hawrysz, A. Godavarty, and E. M. Sevick-Muraca, "Three-dimensional, Bayesian image reconstruction from sparse and noisy data sets: Near-infrared fluorescence tomography," *Proc. Natl. Acad. Sci. U.S.A.* **99**, 9619–9624 (2002).
 30. J. Lee and E. M. Sevick-Muraca, "3-D fluorescence enhanced optical tomography using referenced frequency-domain photon migration measurements at emission and excitation measurements," *J. Opt. Soc. Am. A* **19**, 759–771 (2002).
 31. E. M. Sevick-Muraca, J. P. Houston, and M. Gurfinkel, "Fluorescence-enhanced, near infrared diagnostic imaging with contrast agents," *Curr. Opin. Chem. Biol.* **6**, 642–650 (2002).
 32. V. Ntziachristos and R. Weissleder, "CCD-based scanner for tomography of fluorescent near-infrared probes in turbid media," *Med. Phys.* **29**, 803–809 (2002).
 33. A. Godavarty, M. J. Eppstein, C. Zhang, A. B. Thompson, M. Gurfinkel, S. Theru, and E. M. Sevick-Muraca, "Fluorescence-enhanced optical imaging in large tissue volumes using a gain modulated ICCD camera," *Phys. Med. Biol.* **48**, 1701–1720 (2003).
 34. E. E. Graves, J. Ripoll, R. Weissleder, and V. Ntziachristos, "A sub-millimeter resolution fluorescence molecular imaging system for small animal imaging," *Med. Phys.* **30**, 901–911 (2003).
 35. A. D. Klose and A. H. Hielscher, "Fluorescence tomography with simulated data based on the equation of radiative transfer," *Opt. Lett.* **28**, 1019–1021 (2003).
 36. J. Ripoll, R. Schultz, and V. Ntziachristos, "Free-space propagation of diffuse light: Theory and experiments," *Phys. Rev. Lett.* **91**, 103901–1–4 (2003).
 37. A. B. Milstein, J. J. Stott, S. Oh, D. Boas, R. P. Millane, C. A. Bouman, and K. J. Webb, "Fluorescence optical diffusion tomography using multiple-frequency data," *J. Opt. Soc. Am. A* **21**, 1035–1049 (2004).
 38. V. Ntziachristos, C. Tung, C. Bremer, and R. Weissleder, "Fluorescence-mediated tomography resolves protease activity *in vivo*," *Nat. Med.* **8**, 757–760 (2002).
 39. E. E. Graves, A. Petrovsky, R. Weissleder, and V. Ntziachristos, "In vivo time-resolved optical spectroscopy of mice," *Opt. Soc. Am. Biomed. Opt. Spectroscopy Diagnostics Meeting*, pp. 390–392 (2002).
 40. A. C. Kak and M. Slaney, *Principles of Computerized Tomographic Imaging*, IEEE Press, New York (1988).
 41. H. Xu, H. Dehghani, and B. W. Pogue, "Near-infrared imaging in the small animal brain: optimization of fiber positions," *J. Biomed. Opt.* **8**, 102–110 (2003).
 42. E. E. Graves, J. P. Culver, J. Ripoll, R. Weissleder, and V. Ntziachristos, "Singular-value analysis and optimization of experimental parameters in fluorescence molecular tomography," *J. Opt. Soc. Am. A* **21**, 231–241 (2004).
 43. R. Schultz, J. Ripoll, and V. Ntziachristos, "Non-contact optical tomography of turbid media," *Opt. Lett.* **28**, 1701–1703 (2003).
 44. B. Brooksby, H. Dehghani, B. W. Pogue, and K. D. Paulsen, "Near infrared (NIR) tomography breast image reconstruction with a priori structural information from MRI: algorithm development for reconstructing heterogeneities," *IEEE J. Sel. Top. Quantum Electron.* **9**, 199–209 (2003).
 45. A. D. Klose, V. Ntziachristos, and A. H. Hielscher, "The inverse source problem based on the radiative transfer equation in optical molecular imaging," *J. Comput. Phys.* **202**, 323–345 (2004).